Electrochemical synthesis of titanium dioxide nanostructures and its application in the in dye photocatalytic removal

Electrochemical synthesis of titanium dioxide nanostructures and its application in the in dye photocatalytic removal

P Rivera Bermudez[1], **V Alarcón Rodríguez**[1], **and G Peña-Rodríguez**[1]
[1] Grupo de Investigación en Instrumentación y Física de la Materia Condensada, Universidad Francisco de Paula Santander, San José de Cúcuta, Colombia

E-mail: gabrielpr@ufps.edu.co

Abstract. By electrochemical anodization to titanium sheets, titanium dioxide nanostructures were sintered for 10 V and 20 V and times of 3 hours and 5 hours. For the electrolytic solution, 0.3 g of ammonium fluoride, 97 mL of ethylene glycol and 3 mL of distilled water were used. The sheets (51 mm × 21 mm × 0.4 mm) were treated using abrasive paper and cleaned with a 1:1 solution of ethanol water by means of ultrasound and dried using hot air. A stirring frequency of 300 rpm was used during anodizing. For the sintering of the titanium dioxide anatase phase, heat treatment was applied at 550 °C for 3 hours by means of an electric muffle, with heating speed of 10 °C/min. The crystallinity index, and the quantification of the sintered phases was carried out by means of X-ray diffraction, while the nanoporosities and their distribution were carried out using imageJ software to the images taken by means of scanning electron microscopy. For the photocatalytic treatment of the methylene blue dye in water, the titanium dioxide nanostructures that reported the highest anatase phase were used, where ultraviolet C radiation from a led lamp was applied for 4 direct hours. The efficiency in the removal of the dye was studied by UV-Vis spectrophotometry, finding the highest degradation of the dye for the wavelength of 644 nm.

1. Introduction

In 1971, William Gregor discovered titanium (Ti), a metal that has been widely used in biomedical, metallurgical, and environmental applications among others [1-3]. Titanium dioxide (TiO_2) has mainly three crystalline phases (rutile, anatase and brookite), where nanoparticles or nanostructures (NP) of anatase are the most active and used in cytotoxic and photocatalytic applications [4].

Different experimental techniques have been used for the synthesis of TiO_2 NPs, where the most common are sol-gel, chemical vapor deposition (CVD) and hydrothermal methods, which use high pressures and temperatures, as well as highly toxic chemicals where the cost benefit ratio is unfavorable for scale production [5]. Ecological methods for TiO_2 NPs synthesis have recently been proposed using biological reducing agents for example Verbascum Thapsus plant extracts, which are reproducible on a large scale [6]. There are also numerous low-cost investigations where TiO_2 NPs have been sintered by electrochemical anodization, using Ti and platinum (Pt) electrodes, different electrolytes, and high-potential differences (greater than 30 V), allowing to sinter nanotubes with different morphologies and thicknesses of hundreds of nanometers [7-10]. The application of TiO_2 NPs in photocatalysis using ultraviolet (UV) radiation for the removal of contaminants in water, air and surfaces has been widely used [11-14].

In this work it is presented the TiO_2 NPs synthesis for low voltages, 10 V and 20 V, and times of 3 hours and 5 hours, then the photocatalytic degradation of the dye methylene blue (MB) in water is carried out using the TiO_2 NPs that reported the highest concentration of anatase and the highest crystallinity index.

2. Methodology and materials

For the electrochemical anodization, Ti grade 2 sheets (Ti000233 Goodfellow®) with dimensions of $51\ mm \times 21\ mm \times 0.4\ mm$ were used, which were polished using abrasive paper No. 400, 600, 1200 and 1500, later they were cleaned using ultrasound and solution 1:1 of ethanol-distilled water for 180 seconds and dried using hot air. A 100 mL electrolyte was used, consisting of 97 mL of ethylene glycol (EG), 3 mL of distilled water and 0.3 g of ammonium fluoride (NH4F), which was subjected to magnetic stirring at 500 rpm using the Stirrer plate. Labinco Model L-81 for one hour, the above to homogenize the electrolyte, especially the integration of NH4F with EG and water. For the determination of the pH, TDS, EC of the electrolyte, the Si-Analytics LB 850 multiparameter was used.

The separation of the electrodes was 1 cm, and magnetic stirring was used at 300 rpm for the time of anodization, likewise the electrodes were connected to power source (UNIT-T® UTP3315TFL) for supplying the potential difference of 10 V for 3 hours and 20 V for 5 hours respectively. After the anodizing process, the samples were washed with distilled water, and sonicated through the ultrasound cuvette with the same solution (1:1 ethanol distilled water) for 30 seconds, then they were dried using hot air, and placed in a desiccator with silica gel. Subsequently, the samples were subjected to heat treatment using NEY Vulcan® Model A-550 electric muffle, at 550 °C for 3 hours, with a temperature ramp rate of $10\ °C/min$.

The structural characterization has been done using X-ray diffraction (XRD) (Malvern-PANalytical Empyean Model, CoKα ($\lambda = 1.78901$ Å), 40 KV, range of 20° to 75° of scale 2θ, step of 0.05° and a step time of 0.5 seconds) and the surface morphology by scanning electron microscopy (SEM) (ZEISS RA-ZEI-001 EVO MA 10). In total, ten samples were prepared for each defined voltage and time.

The photocatalysis process was carried out using sintered TiO_2 NPs at 20 V for 5 hours, since they were the ones that reported the highest percentage of crystallinity index and anatase phase of TiO_2, the above was carried out to quantify the removal of the blue dye of MB for a concentration of 20 ppm in water. The direct radiation time was 4 hours, then it was left to rest for 4 days in the photocatalysis cell without the lamp on, to avoid the passage of UV light from a source other than the one used [15].

The Led lamp used was Sylvania (T8, 15 W, $\lambda = 288$ nm) which was placed in a cylindrical PVC cell of 3 inches in diameter and 20 cm in height. For the photocatalysis process, 20 mL of water at 20 ppm with MB deposited in a glass container type Petri dish were used, later two sheets with sintered TiO_2 NPs are immersed on which the radiation cell that the lamp has is placed, and thus start the photocatalysis process. The removal percentage of the MB dye from the waters was studied by the absorbance of the samples before and after the photo-catalytic process, for which the UV-VIS absorption spectrum was recorded using the Thermo Scientific Genesys 10S spectrophotometer, for a wavelength range between 200 nm and 800 nm.

3. Results and discussions

The quantification of the crystalline phases was determined by the Rietveld refinement using the HighScore Plus® software, to the measured XRD pattern. Figure 1 shows the diffraction patterns of the samples with the phases identified as a product of the refinement carried out, where M1 corresponds to the sample sintered at $10\ V - 3$ hours, M2 at $10\ V - 5$ hours, M3 the one treated at $20\ V - 3$ hours and M4 at $20\ V - 5$ hours. It is observed that the TiO_2 phases formed were anatase and rutile, as well as the titanium phase (Ti_2) and finally the iron oxide phase (Fe_3O_4) was also found.

The previous results are consistent with those reported in the literature, where it is established that between 25° to 30° in 2θ is the reflection of the plane (101) of anatase which corresponds to the preferential orientation along this plane of the α-Ti phase, as well as the maximum intensity reflection corresponding to Ti_2, is due to the substrate or sheet of Ti [16]. On the other hand, it is observed that as

the potential difference and time increase in the anodizing process, the peak corresponding to the anatase phase increases its intensity, while the peak corresponding to Ti_2 remains practically constant.

The observed in Figure 1 is consistent with the reported by [17], who studied the growth behavior of TiO_2 nanotubes by electrochemical anodizing, confirming that during the first 30 minutes of heat treatment, the initial nucleation of small amounts of anatase is formed, and that after this time the rutile is sintered, likewise that after the first hour, an evolution of the reflection peaks appears in the range of $2\theta = 38°$ to $2\theta = 45°$, which in fact corresponds to the superposition of the anatase and Ti_2 peaks, after this time the thickness of the layer increases and the nanometric tubular structures are formed. On the other hand, it is observed that the mean width of the reflection peaks is narrow, which indicates that the oxide layer formed is polycrystalline.

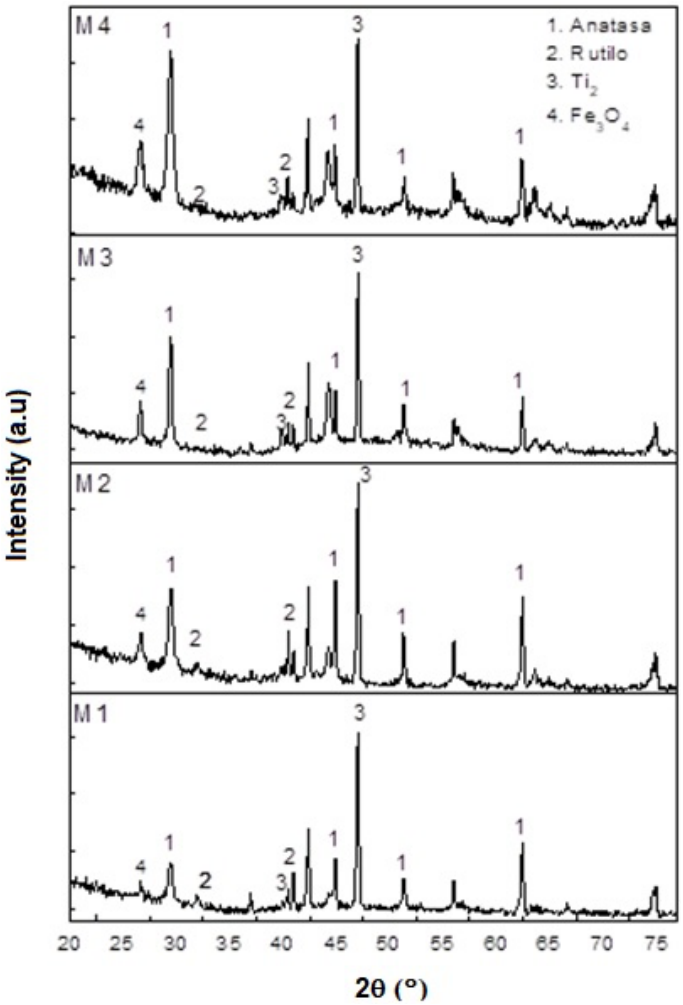

Figure 1. XRD diffraction patterns of the samples.

To determine the percentage of the crystallinity index (%CI), the method reported by [18] were used, which consists of taking the intensity of the crystalline plane of greatest reflection (I_{max}) corresponding to the crystalline phase of interest, and the intensity of the amorphous part of said plane of reflection (I_{min}), both measured with respect to a horizontal line at the base of the reflection peak under study. Then, %CI is determined by applying Equation (1).

$$\%CI = \left(\frac{I_{max} - I_{min}}{I_{max}}\right) * 100. \quad (1)$$

The %CI is presented in Table 1, in this the sample with the highest %CI is M4, which corresponds to the sample that reported the highest concentration of the anatase phase of TiO_2. Initially during the anodization process a TiO_2 barrier grows formed by the interaction of the metal with the OH^- or O^{2-} ions, product of the electric field existing between the electrodes [19], later when the growth rate of the titanium dioxide layer on the anode surface is balanced with the dissolution rate of the oxide formed in the TiO_2/electrolyte interface, the thickness of the layer practically remains constant [20].

Table 1. % CI of the samples.

Samples	%CI
M1	42.57
M2	56.06
M3	66.03
M4	67.33

Table 2. Percentage of discoloration and efficiency of the water samples with dye MB.

λ (nm)	Abs_{before}	Abs_{after}	% Disc.	% Efficiency
664	1.451	0.404	72.15	41.1
613	0.811	0.225	72.25	-
292	0.743	0.346	53.43	-

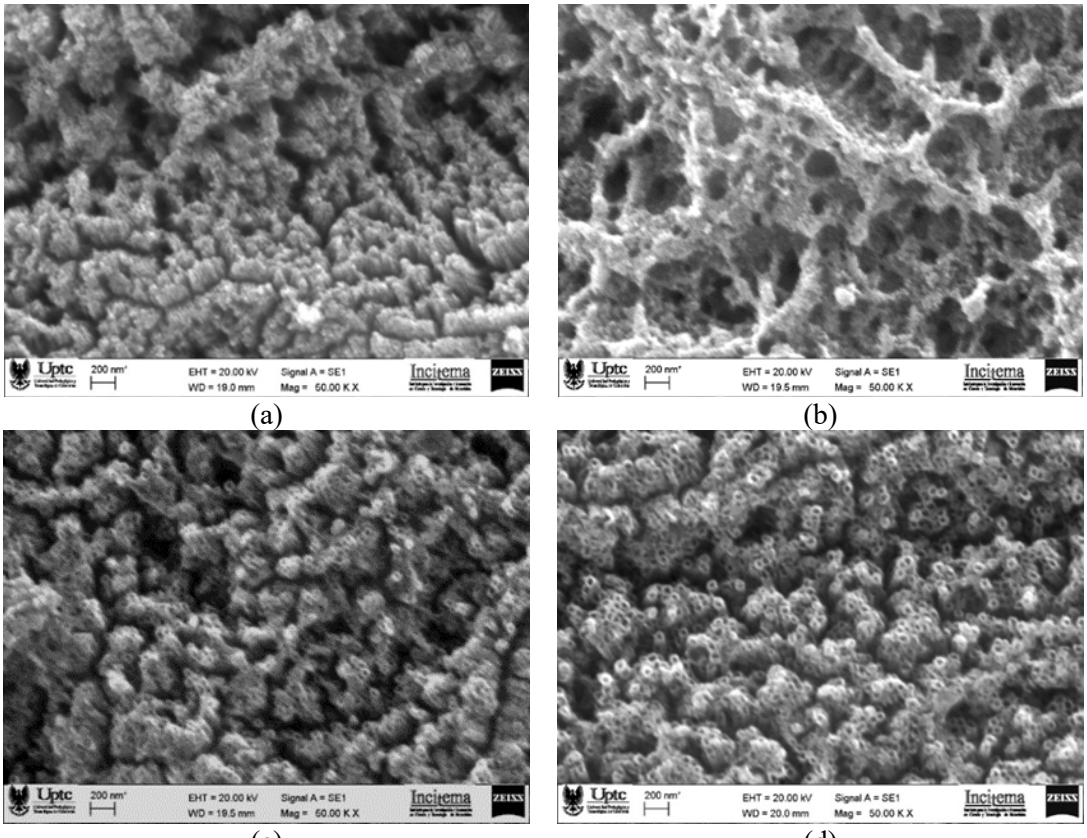

Figure 2. SEM images at 50 KX for sintered samples. (a) M1; (b) M2; (c) M3; (d) M4.

The morphology of the sintered nanostructures using SEM for a magnification at 50 KX is presented in Figure 2, which an irregular topography of nano-cracks that furrow nanostructures in a tubular shape can be seen; on the other hand, it is evidenced for the sintered sample at 10 V and 5 hours that the morphology is very heterogeneous and amorphous, showing that for a voltage of 10 V the best formation time of the TiO_2 NPs was 3 hours, which is consistent because at shorter times the surface current density is higher, allowing the organized formation of the nanostructures [21].

Also, when comparing the morphology of the samples sintered at 10 V with those anodized at 20 V, it is evidenced that by increasing the voltage the morphology is better, and the nano-porosities are better resolved, which is consistent with what has been reported, where they state that for potential differences

greater than 20 V, both the diameter and the length of the nanostructures depend linearly with the potential difference, presenting self-assembled morphologies [21].

In general, it can be affirmed that the samples that present a better morphology are those sintered at 20 V for 5 hours, which according to the XRD analysis, are those that present the best crystallinity index and the highest anatase phase formation, finding an average size of the porosities of 39.05 nm, it was also evidenced that as the time increased from 3 hours to 5 hours, the size of the porosities decreased by approximately 33%, and that these values are found in the ranges reported by the literature [22-23].

However, a tubular morphology was not observed, due to the low potential difference used during anodization. The thicknesses of the sintered NPs were found using Mitutoyo digital micrometer, where the thickness of the Ti sheet was measured before and after the anodization process, finding for M1 it was 7.916 ± 0.134 µm; for M2 it was 15.225 ± 0.456 µm; for M3 it was 448.750 ± 14.567 µm and for M4 it was 953.752 ± 23.438 µm. From the above, it can be inferred that as the potential difference and the anodization time increase, the thickness of the anodized oxide layer increases [24].

In Figure 3, the UV/VIS absorption spectrum is presented for a wavelength range of 200 nm to 800 nm of the water samples with dye MB before and after the photocatalytic process, in this the characteristic peaks of dye MB are observed ($\lambda = 613$ nm, $\lambda = 664$ nm and $\lambda = 292$ nm) [25]; on the other hand, it is evidenced that the maximum absorbance occurs for $\lambda = 664$ nm, being consistent with that reported in the literature [26-28].

The maximum absorbance corresponds to the monomers present in the dye MB, through the aromatic rings that can be replaced by sulfur or nitrogen according to the molecular structure of the dye MB, likewise the shoulder present at $\lambda = 613$ nm is due to the dye attenuation, while the absorbance due to benzene rings is observed for $\lambda = 292$ nm. To perform the calibration of the dye MB concentration, samples with concentrations of 20 mg/L, 40 mg/L, 50 mg/L and 60 mg/L were prepared, and the absorbances were measured for $\lambda = 664$ nm, in the Figure 4, the best linear adjustment to the experimental data of the absorbances (y) versus concentration (x) of dye MB is presented.

In Table 2, the discoloration percentages (% Disc.) are presented using the absorbances for the three peaks of the absorption spectrum, which were found using linear fit (see Figure 4); from these it is observed that the photocatalytic oxidation for wavelength of $\lambda = 664$ nm, $\lambda = 613$ nm corresponding to the monomers present in MB [29], the percentage of discoloration (% Disc.) was practically the same (~72%), while for wavelength $\lambda = 292$ nm, which corresponds to the benzene rings, this percentage decreases in 53.43%.

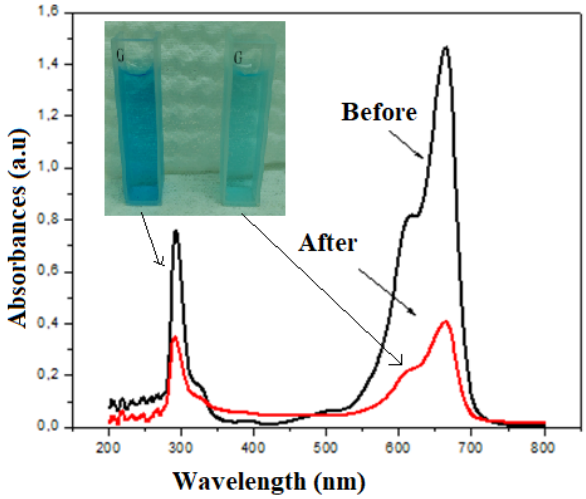

Figure 3. UV-VIS absorption spectrum for the MB water sample before and after the photocatalytic treatment.

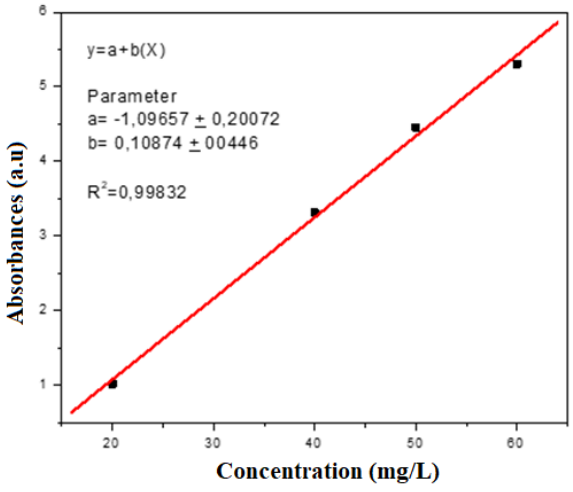

Figure 4. Best linear fit to the absorbance vs. concentration data ($\lambda = 664$ nm), for the dye MB.

On the other hand, to calculate the percentage of efficiency (% Efficiency) in the remotion of dye MB, the data of the linear adjustment was used (see Figure 4), which was carried out for the wavelength of 664 nm, finding an efficiency in removal of dye MB of the 41.1%, which are greater than those found using TiO_2 nanotubes anodized at greater potential differences [15,19]. In general, it is evident from the results presented that the TiO_2 NPs sintered by anodization with a potential difference of 20 V at 5 hours are efficient in the photocatalytic removal of dye MB in water.

4. Conclusions

It was possible to sinter titanium dioxide nanoparticles by electrochemical anodization of titanium grade 2 sheets using an electrolyte based on ethylene glycol and ammonium fluoride for low potential differences 10 V and 20 V and times of 3 hours and 5 hours, finding that the samples sintered at 20 V and 5 hours were those that presented the highest percentage of the crystallinity index, and the highest anatase phase concentration, with a morphology formed by nano-porosities with thicknesses of hundreds of microns that increase with increasing potential difference and anodization time. The study by UV/VIS absorption spectrophotometry in the removal of methylene blue in water for a concentration of 20 ppm using ultraviolet C photocatalysis ($\lambda = 288$ nm), and the titanium dioxide nanostructures sintered at 20 V for 5 hours, reported an efficiency in the degradation of the colorant of the order of 72%, and a decrease in the concentration of dye methylene blue around 41.1%.

References

[1] Baan R, Straif K, Grosse Y, Secretan B, El Ghissassi F, Cogliano V 2006 Carcinogenicity of carbon black, titanium dioxide, and talc *The Lancet Oncology* **7(4)** 295
[2] Bavykin D V, Friedrich J M, Walsh F C 2006 Protonated titanates and TiO2 nanostructured materials: synthesis, properties, and applications *Advanced Materials* **18(21)** 2807
[3] McCullagh C, Robertson J M, Bahnemann D W, Robertson P K 2007 The application of TiO2 photocatalysis for disinfection of water contaminated with pathogenic micro-organisms: a review *Research on Chemical Intermediates* **33(3–5)** 359
[4] Vandebriel R J, Vermeulen J P, van Engelen L B, de Jong B, Verhagen L M, de la Fonteyne-Blankestijn L J, Hoonakker M E, de Jong W H 2018 The crystal structure of titanium dioxide nanoparticles influences immune activity in vitro and in vivo *Particle and Fibre Toxicology* **15(1)** 9
[5] Jafari S, Mahyad B, Hashemzadeh H, Janzafa S, Gholikhani T, Tayebi L 2020 Biomedical applications of TiO_2 nanostructures: recent advances *International Journal of Nanomedicine* **15** 3447
[6] Esfahani R N, Khaghani S, Azizi A, Mortazaeinezhad F, Gomarian M 2020 Facile and eco-friendly synthesis of TiO_2 NPs using extracts of *Verbascum thapsus* plant: an efficient photocatalyst for reduction of Cr (VI) ions in the aqueous solution *Journal of the Iranian Chemical Society* **17(1)** 205
[7] Damas Resende P, Rabelo Junqueira R M, Dornelas Silva J, Azevedo Lopes N I, Arruda Santos L, Lopes Buono V T 2020 Comparative study of nanostructured titania grown by electrochemical anodization of α-Ti and β-TiNi substrates in organic electrolytes *Journal of Materials Research and Technology* **9(5)** 10121
[8] Gong D, Grimes C A, Varghese O K, Hu W, Singh R S, Chen Z, Dickey E C 2001 Titanium oxide nanotube arrays prepared by anodic oxidation *Journal of Materials Research* **16(12)** 3331
[9] Yoo H, Kim M, Kim Y-T, Lee K, Choi J 2018 Catalyst-doped anodic TiO_2 nanotubes: binder-free electrodes for (photo)electrochemical reactions *Catalysts* **8(11)** 555
[10] Yung-Huang C, Yuan-Tsung C, Chien-Sheng H, Chia-Ling L, Shih-Hung L, Bohr-Ran H, Chih C 2018 Growth mechanism of self-assembled Ti_xW_yO nanotubes fabricated by TiW alloy anodization *Journal of The Electrochemical Society* **165(10)** D477
[11] Katal R, Masudy-Panah, S, Tanhaei M, Farahani M H, Jiangyong, H 2020 A review on the synthesis of the various types of anatase TiO_2 facets and their applications for photocatalysis *Chem. Eng. J.* **384** 123384
[12] Bingham M, Mills A 2020 Photonic efficiency, and selectivity study of M (M = Pt, Pd, Au and Ag)/TiO2 photocatalysts for methanol reforming in the gas phase *J. Photochem. Photobiol. A Chem.* **389** 112257
[13] Tarcea C I, Pantilimon C M, Matei E, Predescu A M, Berbecaru A C, Rapa M, Turcanu A, Predescu C 2020 Photocatalytic degradation of methylene blue dye using TiO_2 and $Fe_3O_4/SiO_2/TiO_2$ as photocatalysts *IOP Conf. Series: Materials Science and Engineering* **877** 012008

[14] Bakbolat B, Daulbayeb C, Sultanov F, Beissenov R, Umirzakov A, Mereke A, Bekbaev A, Chuprakov I 2020 Recent developments of TiO_2-based photocatalysis in the hydrogen evolution and photodegradation: a review *Nanomaterials* **10** 1790
[15] Torres López C 2013 *Fotocatálisis en Nanotubos Metaestables de TiO_2 Sobre Electrodos de Ti para la Degradación de Naranja de Metilo* (Querétaro: Centro de Investigación y Desarrollo Tecnológico en Electroquímica)
[16] Sopha H, Norikawa Y, Motola M, Hromadko L, Rodriguez J, Cerny J, Nohira T, Yasuda K, Macak J 2020 Anodization of electrodeposited titanium films towards TiO_2 nanotube layers *Electrochemistry Communications* **118** 106788
[17] Siampiringue M, Massard C, Caudron E, Sibaud Y, Sarakha M, Awitor K 2016 Impact of annealing treatment on the behaviour of titanium dioxide nanotube layers *Journal of Biomaterials and Nanobiotechnology* **7** 142
[18] Park S, Baker J, Himmel M, Parilla P, Johnson D 2010 Cellulose crystallinity index: measurement techniques and their impact on interpreting cellulase performance *Biotechnology for Biofuels* **3** 10
[19] Dubed Bandom G 2017 *Síntesis y Caracterización Fisicoquímica y Fotoelectroquímica de Membranas de Nanotubos de TiO_2 (MNTs-TiO_2) Modificadas con Materiales Electrocatalíticos* (Querétaro: Centro de Investigación y Desarrollo Tecnológico en Electroquímica)
[20] Reynaud Morales A G, Cuevas Arteaga C 2013 Preparación de nanoestructuras porosas de TiO_2 por anodización a bajo potencial en electrólito acuoso de CH_3COOH/HF *Superficies y Vacío* **26(2)** 64
[21] Concha Guzmán M O, Reynaud Morales A G, Cuevas Arteaga C, Rincón González M E 2010 Crecimiento de nanoestructuras de TiO_2 obtenidas a bajo potencial por reacción anódica en soluciones ácidas H_2SO_4/HF *Superficies y Vacío* **23(S)** 183
[22] Hoseinzadeh T, Ghorannevis Z, Ghoranneviss M, Sari A, Salem M 2017 Effects of various applied voltages on physical properties of TiO_2 nanotubes by anodization method *J. Theor. Appl. Phys.* **11** 243
[23] Michalska-Domanska M, Łazinska M, Łukasiewicz J, Mol J, Durejko T 2020 Self-organized anodic oxides on titanium alloys prepared from glycol- and glycerol-based electrolytes *Materials* **13** 4743
[24] Chernozem R V, Surmeneva M A, Surmenev R A 2016 Influence of anodization time and voltage on the parameters of TiO_2 nanotubes *IOP Conf. Series: Materials Science and Engineering* **116** 012025
[25] Nosrati R, Olad A, Shakoori S 2017 Preparation of an antibacterial, hydrophilic and photocatalytically active polyacrylic coating using TiO_2 nanoparticles sensitized by graphene oxide *Materials Science and Engineering C* **80** 642
[26] Xiong X, Tian R, Lin X, Chu D, Li S 2015 Formation and photocatalytic activity of $BaTiO_3$ nanotubes via hydrothermal process *Journal of Nanomaterials* **16(1)** 173
[27] Dinh V P, Huynh T D, Le H M, Nguyen V D, Dao V A, Hung N Q, Tuyen L A, Lee S, Yi J, Nguyen T D, Tan L V 2019 Insight into the adsorption mechanisms of methylene blue and chromium (III) from aqueous solution onto pomelo fruit pee *Royal Society of Chemistry Advances* **9** 25847
[28] Tardivo J P, Del Giglio A, Santos de Oliveira C, Santesso Gabrielli D, Couto Junqueira H, Batista Tada D, Severino D, de Fatima Turchiello R, Baptista M 2005 Methylene blue in photodynamic therapy: from basic mechanisms to clinical application *Photodiagnosis and Photodynamic Therapy* **2** 175
[29] Vásquez A L, Almanza O, Acosta M F, Tio B O 2016 Degradación fotocatalítica de contaminantes orgánicos presentes en agua residual de la industria litográfica mediante oxido de bismuto(III)/oxido de titanio (Bi2O3/TiO2) *Información Tecnológica* **27(1)** 147